

This is an Open Access document downloaded from ORCA, Cardiff University's institutional repository: <https://orca.cardiff.ac.uk/id/eprint/93767/>

This is the author's version of a work that was submitted to / accepted for publication.

Citation for final published version:

Pelayo Garcia de Arquer, F., Beck, Fiona J., Bernechea, Maria and Konstantatos, Gerasimos 2012. Plasmonic light trapping leads to responsivity increase in colloidal quantum dot photodetectors. *Applied Physics Letters* 100 (4), 043101. 10.1063/1.3678039

Publishers page: <http://dx.doi.org/10.1063/1.3678039>

Please note:

Changes made as a result of publishing processes such as copy-editing, formatting and page numbers may not be reflected in this version. For the definitive version of this publication, please refer to the published source. You are advised to consult the publisher's version if you wish to cite this paper.

This version is being made available in accordance with publisher policies. See <http://orca.cf.ac.uk/policies.html> for usage policies. Copyright and moral rights for publications made available in ORCA are retained by the copyright holders.



Plasmonic light trapping leads to responsivity increase in colloidal quantum dot photodetectors

F. Pelayo García de Arquer, Fiona J. Beck, María Bernechea, and Gerasimos Konstantatos

Citation: *Appl. Phys. Lett.* **100**, 043101 (2012); doi: 10.1063/1.3678039

View online: <http://dx.doi.org/10.1063/1.3678039>

View Table of Contents: <http://apl.aip.org/resource/1/APPLAB/v100/i4>

Published by the [American Institute of Physics](http://www.aip.org).

Related Articles

Fully programmable single-photon detection module for InGaAs/InP single-photon avalanche diodes with clean and sub-nanosecond gating transitions

Rev. Sci. Instrum. **83**, 013104 (2012)

Photovoltaic quantum dot quantum cascade infrared photodetector

Appl. Phys. Lett. **100**, 021105 (2012)

Extended spectral response in organic photomultiple photodetectors using multiple near-infrared dopants

APL: Org. Electron. Photonics **5**, 9 (2012)

Extended spectral response in organic photomultiple photodetectors using multiple near-infrared dopants

Appl. Phys. Lett. **100**, 013309 (2012)

Leaky-mode effects in plasmonic-coupled quantum dot infrared photodetectors

Appl. Phys. Lett. **100**, 011110 (2012)

Additional information on *Appl. Phys. Lett.*

Journal Homepage: <http://apl.aip.org/>

Journal Information: http://apl.aip.org/about/about_the_journal

Top downloads: http://apl.aip.org/features/most_downloaded

Information for Authors: <http://apl.aip.org/authors>

ADVERTISEMENT

**AIP**Advances

Submit Now

**Explore AIP's new
open-access journal**

- **Article-level metrics
now available**
- **Join the conversation!
Rate & comment on articles**

Plasmonic light trapping leads to responsivity increase in colloidal quantum dot photodetectors

F. Pelayo García de Arquer, Fiona J. Beck, María Bernechea, and Gerasimos Konstantatos^{a)}
ICFO-Institut de Ciències Fotoniques, Mediterranean Technology Park, 08860 Castelldefels, Barcelona, Spain

(Received 4 November 2011; accepted 22 December 2011; published online 23 January 2012)

We report broadband responsivity enhancement in PbS colloidal quantum dot (CQDs) photoconductive photodetectors due to absorption increase offered by a plasmonic scattering layer of Ag metal nanoparticles. Responsivity enhancements are observed in the near infrared with a maximum 2.4-fold increase near the absorption band edge of $\sim 1 \mu\text{m}$ for $\sim 400 \text{ nm}$ thick devices. Additionally, we study the effect of the mode structure on the efficiency of light trapping provided by random nanoparticle scattering in CQD films and provide insights for plasmonic scattering enhancement in CQD thin films. © 2012 American Institute of Physics. [doi:10.1063/1.3678039]

Quantum dot photodetectors have emerged as a promising top-surface photodetector technology readily integrated on complementary metal–oxide–semiconductors platforms for low-cost near infrared sensing.^{1–4} Colloidal quantum dots (CQDs) have attracted significant attention in view of their solution-processability and bandgap tunability extended from the visible to the infrared in the case of PbS CQDs. Colloidal quantum dot photoconductive detectors^{4,5} and photodiodes⁶ with very high sensitivities have been reported and CQD solar cells^{7–9} with efficiencies over 6% demonstrate the potential of this emerging technology.¹⁰ PbS CQDs offer high absorption coefficients $\sim 10^5 \text{ cm}^{-1}$ in the visible yet their absorption coefficient near their band edge is $\sim 10^4 \text{ cm}^{-1}$. Therefore, films of $\sim 1 \mu\text{m}$ are required to fully absorb incident light. However, carrier lifetime and mobility in these films pose a restriction in thickness for efficient carrier extraction on the order of 400–500 nm.¹¹ In photoconductive detectors, further enhancement in sensitivity can be achieved by employing thinner absorbing layers in view of the dark current reduction and reduced generation-recombination noise.¹² Light trapping schemes to increase absorption in the active layer can offer the possibility to overcome these challenges towards more efficient QD solar cells and more sensitive photodetectors.

Plasmonics provide effective light trapping for a variety of semiconductor devices.^{13,14} Light trapping schemes based on far-field scattering from metal nanostructures^{15,16} on silicon solar cells and on near field enhancements from embedded metal nanoparticles (MNPs) in polymer solar cells,¹⁷ have been reported. In particular, islandised Ag films have shown to effectively scatter and couple light into trapped modes in underlying thick silicon semiconductor films.¹⁵ However, this mechanism of light trapping based on plasmonic MNPs has not yet been explored in thin film devices based on colloidal quantum dots.

In this paper, we employ a plasmonic scattering layer to demonstrate the benefits of light trapping for colloidal quantum dot optoelectronics. The MNP films have scattering resonances near the exciton peak when embedded in the PbS-CQD layer, and are located on the rear of the device in

order to maximize the scattering of light¹⁸ and to avoid losses associated with Fano interference.¹⁹ We demonstrate broadband responsivity enhancements at wavelengths beyond 600 nm with a maximum 2.4-fold increase near the absorption band edge of PbS quantum dots with first exciton peak at 950 nm. Furthermore, we investigate the importance of the device thickness in utilizing plasmonic light trapping from random MNP arrays due to reduced mode density in thin CQD PbS films.

Figure 1(a) shows the device structure under study. Inter-digited Au electrodes define a device area of $10 \mu\text{m}$ by 3 mm , with an electrode height of 300 nm . The islandised Ag films were fabricated on the glass substrates with pre-patterned Au electrodes by evaporation of 15 nm of Ag, followed by a 1 h annealing at 250°C in a N_2 atmosphere. Upon heating, the film coalesces into discrete MNPs between

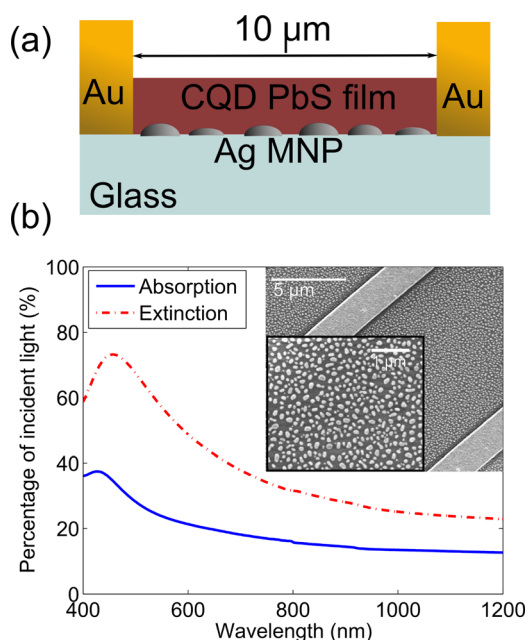


FIG. 1. (Color online) (a) Schematic of the photodetector device structure showing embedded nanoparticles. (b) Absorption and extinction spectra of nanoparticles on glass and micrographs of Ag islandised films formed between the Au contacts before CQD PbS deposition, showing the size and shape distribution of the Ag nanoparticles (inset).

^{a)}Electronic mail: gerasimos.konstantatos@icfo.es.

the contacts, as shown in Fig. 1(b) (inset). The films were characterized by scanning electron microscopy (SEM) and atomic force microscopy (AFM). The MNPs were found to have a “flattened” hemispherical shape, an average diameter of 100 nm, a height of 30 nm, and a surface coverage of 31%. The measured absorption and extinction of the MNPs on glass is shown in Fig. 1(b), clearly showing the broad localized surface plasmon resonance peak at a wavelength of 460 nm. PbS CQD films were deposited over the electrodes in ambient conditions using a layer by layer (LbL) procedure.²⁰ Air stability as well as surface passivation of the QDs are provided by ethanedithiol, a cross-linking ligand which leads to robustly passivated PbS QD surfaces.^{21,22}

When embedded in CQD PbS films, the optical properties of the Ag MNPs change due to the relatively high refractive index of the semiconductor. To characterize the scattering behavior of the MNP films once embedded in the PbS CQD films, finite-difference time domain (FDTD) simulations were performed. Simulations of single particles allow the calculation of the scattering cross-section (Q_{scat})²³ and have been shown to compare well to experimentally measured results for Ag islanded films.¹⁹ Single Ag nanoparticles with a “flattened” hemispherical shape, a height of 30 nm and a diameter of 100 nm were modeled embedded in a semi-infinite PbS film on a glass substrate, corresponding to the average size and geometry of the nanoparticles observed experimentally. Dielectric constants for CQD PbS films were modeled using an effective medium method.²⁴ For Ag, the dielectric constants were modeled using data from Johnson and Christy. Clear peaks in the scattering cross-section spectra occur at the surface plasmon resonance $\lambda_{\text{SPR}} = 840$ nm, with a maximum value of $Q_{\text{scat}} = 8$.²⁰ This suggests that, for a surface coverage of 31%, a large fraction of the incident light should be scattered by the particles at wavelengths close to the exciton peak of the CQDs, at $\lambda = 950$ nm. For the experimental MNP films under study, which have a roughly Gaussian size distribution about the average diameter of 100 nm, much broader scattering and absorption cross section peaks would be expected, extending to wavelengths near the band-edge of the PbS QDs.

Three different CQD PbS film thicknesses were studied with and without embedded Ag MNPs. The thicknesses for the two classes of devices (with and without MNP) were found to be, $t = 190$ nm, 330 nm, and $420 \text{ nm} \pm 10$ nm. Figure 2(a) shows the measured responsivity, with and without embedded MNP films, for different device thicknesses. For samples without MNPs, the responsivity increases with thickness due to an increase in absorption. The introduction of embedded MNPs reduces the responsivity for $\lambda < 700$ nm for the thinnest device ($t = 190$ nm). Figure 2(b) shows the responsivity (R) enhancement, defined as the ratio of R with MNPs over R without MNP for samples of the same thickness, calculated from the data of Fig. 2(a). Responsivity is significantly enhanced around $\lambda = 800$ nm, and beyond $\lambda > 1000$ nm due to the presence of the MNPs. For the thinnest device ($t = 190$ nm), the enhancement is as high as 50% for $\lambda > 1000$ nm, as the absorption in the CQD PbS films reduces and light trapping becomes more critical. For thicker devices, significant enhancement occurs at shorter wavelengths, which reaches 40% for $t = 420$ nm at $\lambda = 800$ nm,

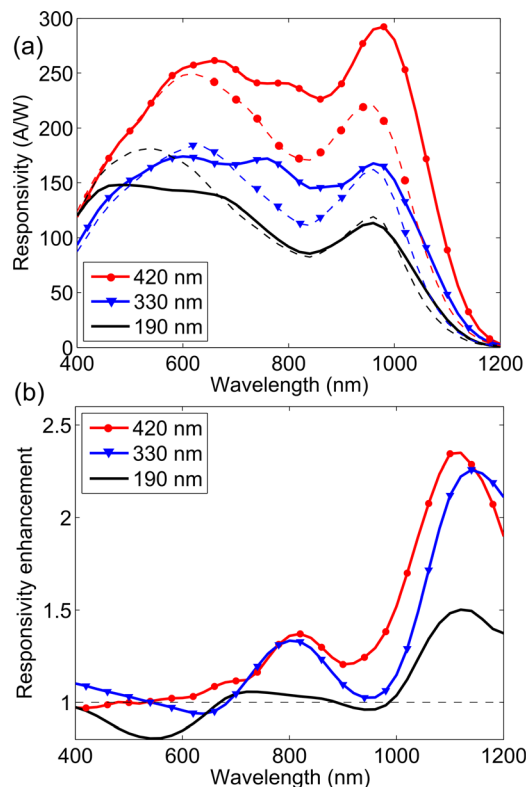


FIG. 2. (Color online) Responsivity (a) and responsivity enhancement (b) of the three different thicknesses photoconductive detectors at 10 V (10 kV/cm). Spectra are shown for samples with (solid lines) and without (dashed lines) embedded Ag MNPs.

near the scattering resonance of the MNP films, as estimated from FDTD simulations. For $\lambda > 1000$ nm, larger enhancements of up to 130% and 140% are observed for $t = 330$ nm and $t = 420$ nm, respectively.

Using the same procedure, CQD films were spin casted on $20 \text{ mm} \times 20 \text{ mm}$ glass slides for reflection and transmission measurements to monitor the absorption enhancement in the presence of Ag MNPs at different thickness of PbS layers. Figure 3(a) shows the absorption and (b) the absorption enhancement (defined as the ratio of absorption with MNPs over the absorption in neat PbS-CQDs films) for different film thicknesses on glass. The spectra of the MNPs embedded in the PbS-CQD include absorption in both the semiconductor and the MNPs themselves. At long wavelengths, near the band edge of the PbS-CQD where the absorption in the semiconductor is very low, the measured absorption occurs mainly in the nanoparticle film, which has a broad extinction resonance. Additionally, light scattered into guided modes in the PbS-CQD film that is not absorbed at long wavelengths can be guided to the edge of the sample and lost. This can also occur for the thicker reference samples as the large area optical samples become increasingly rough with increasing thickness, over the large area samples considered in this measurement.

Absorption enhancements show similar spectral behavior compared to responsivity enhancements, peaking at wavelengths near the MNPs resonance and increasing for longer wavelengths. However, a different trend appears with thickness, as enhancements in absorption decreases with increasing film thickness, while responsivity enhancements increase

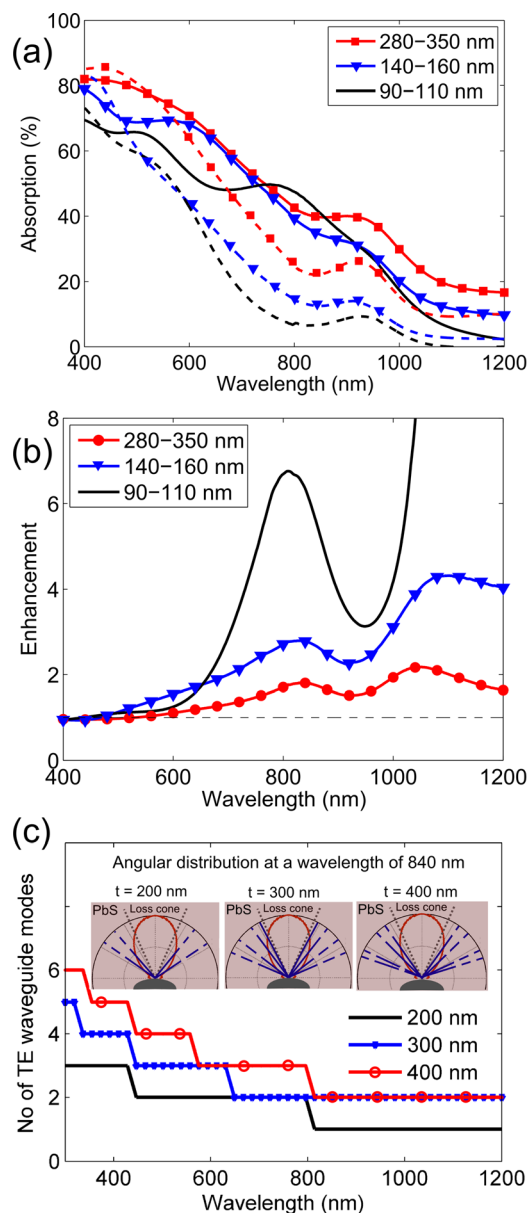


FIG. 3. (Color online) Absorption (a) and absorption enhancement (b) of PbS-CQD films on glass for three different thicknesses. Spectra are shown for samples with (solid lines) and without (dashed lines) embedded Ag MNPs. (c) Number of TE modes in a planar PbS-CQD film in air, calculated at each wavelength for different film thicknesses (an equivalent calculation can be performed for TM modes, giving similar results). (Inset) The calculated angular distribution of light scattered at resonance ($\lambda_{\text{SPR}} = 840$ nm) by a single, flattened Ag hemisphere with $d = 100$ nm and $h = 30$ nm (solid lines), compared to the propagation angles for allowed TE and TM modes in the PbS-CQD waveguide for different thicknesses (broken lines), at the same wavelength. The loss cone for a PbS-CQD/air interface is also shown (dotted lines).

with thickness. To investigate the differences in the enhancement of absorption and responsivity trends with thickness, we consider the mode structure in the PbS film. In order to estimate how efficiently light is coupled into trapped modes propagating in the PbS-CQD films by scattering from the Ag MNPs, we compare the scattering distribution of the MNPs with the propagation angles of modes in the PbS-CQD film. The scattering distribution of a single hemispherical Ag MNP ($d = 100$ nm, $h = 30$ nm), embedded in a semi-infinite PbS CQD film is calculated from FDTD simulations, as described in Ref. 23. Additionally, the waveguide modes of thin

PbS-CQD films in air were calculated in a simple manner by finding solutions to the self-consistency condition.²⁵

Figure 3(c) shows the number of TE modes that exist in the PbS-CQD film at each wavelength, calculated as $M = \frac{2t}{\lambda} \sqrt{n_{\text{PbS-CQD}} - n_{\text{air}}}$, for different film thicknesses. An equivalent calculation can be performed for TM modes, yielding similar results. For $\lambda > 800$ nm, the $t = 200$ nm PbS-CQD film is in single mode operation (i.e., only one TE and one TM mode exists), but for thicker films of $t = 300$ nm and 400 nm, higher order waveguide modes can propagate at these wavelengths. The angular distribution of light scattered by the MNP at resonance ($\lambda_{\text{SPR}} = 840$ nm) is plotted in the insets (solid lines) and compared to the propagation angles of the modes that exist at the same wavelength for films with $t = 200$ nm, 300 nm, and 400 nm (broken lines). The loss cone for an air/PbS-CQD interface is also shown with a dashed grey line. For $t = 200$ nm, only one TE and one TM mode exist, and these are propagating at high angles, reducing the efficiency of coupling to these modes with Ag MNP scattering and, therefore, reducing the amount of light trapped in the waveguide for this film thickness. For $t = 300$ and $t = 400$ nm, there are two possible TE and two possible TM modes, some which propagate at smaller angles, allowing more efficient coupling of light scattered by the Ag MNP. These modeling results agree qualitatively with the experimentally measured responsivity enhancements at $\lambda > 800$ nm shown in Fig. 2(b), which demonstrate a significantly lower enhancement for the $t = 190$ nm case (in single mode operation), compared to the thicker films (with propagating higher order modes). Additionally, for films with $t = 300$ nm and 400 nm, the mode distributions shown in the insets in Fig. 3 are similar at $\lambda = 840$ nm, implying that similar enhancements in absorption would be expected, in agreement with measured responsivity enhancements.

We now compare our plasmonic light trapping with the enhancement offered by a back-reflector to show further performance improvement offered by efficient plasmonic light trapping in the presence of a mirror. Figure 4 shows the measured responsivity of the device with $t = 420$ nm with and without embedded MNPs, in the presence of a back-reflector. A glass slide coated with 200 nm of Ag was used as a reflector, with a measured reflection of above 90% in the 400 - 1200 nm region. Responsivity enhancement of 92% is achieved by employing back-reflector, whereas an over 84% extra enhancement is achieved by the synergism of the back-reflector with plasmonic MNPs due to enhanced an increase in the fraction of the light scattered by the MNPs scattered into the PbS-CQD film,²⁶ and two-fold increase on the number of modes in the presence of the mirror.

In conclusion, we have demonstrated that scattering by embedded Ag MNPs offers broadband responsivity enhancements in thin CQDs PbS photoconductive photodetectors. A maximum 2.4-fold enhancement factor was obtained near PbS-QDs bandgap, increased to a 3.6-fold when combined with a back reflector. We attribute this photocurrent increase to increased absorption due to scattering from MNPs into trapped modes inside the CQDs PbS film. We demonstrate that the mode structure of the film has to be taken into account in maximizing the coupling between the light scattered by the MNP and propagating modes inside the active layer. Applying

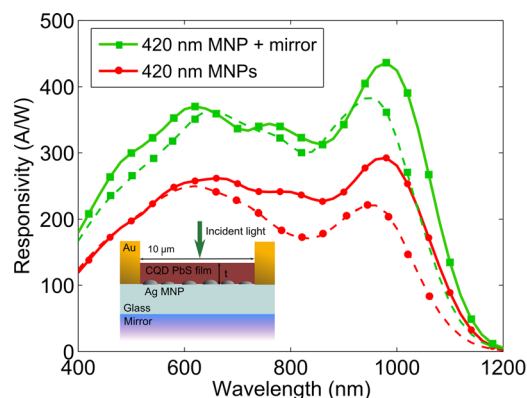


FIG. 4. (Color online) Responsivity of 420 nm thick devices with and without mirror (square and circle marked lines, respectively) with and without MNPs (solid and dashed lines, respectively) measured at 10 V bias. The inset shows a schematic of the measurement with mirror.

a reflector underneath the MNPs increases the responsivity enhancements further, due to an increase in both the number of modes at long wavelengths and the efficiency of light scattering into the active layer. The narrow radiation pattern of Ag MNPs embedded in PbS CQDs film limits the light that can be coupled into the film as only a fraction of the scattered light is traveling at high angles capable of coupling efficiently to trapped waveguide modes.²⁷ The absorption enhancement demonstrated here could be significantly improved by designing periodic nanostructures that couple preferentially to waveguide modes in the active region.

This research has been partially supported by Fundació Privada Cellex Barcelona. We also acknowledge support from European Commission's Seventh Framework Programme for Research under contract PIRG06-GA-2009-256355.

¹S. Cosentino, P. Liu, S. T. Le, S. Lee, D. Paine, A. Zaslavsky, D. Pacifici, S. Mirabella, M. Miritello, I. Crupi *et al.*, *Appl. Phys. Lett.* **98**, 221107 (2011).

²J. M. Shieh, W. C. Yu, J. Y. Huang, C. K. Wang, B. T. Dai, H. Y. Jhan, C. W. Hsu, H. C. Kuo, F. L. Yang, and C. L. Pan, *Appl. Phys. Lett.* **94**, 241108 (2009).

- ³J. M. Shieh, Y. F. Lai, W. X. Ni, H. C. Kuo, C. Y. Fang, J. Y. Huang, and C. L. Pan, *Appl. Phys. Lett.* **90**, 051105 (2007).
- ⁴G. Konstantatos, I. Howard, A. Fischer, S. Hoogland, J. Clifford, E. Klem, L. Levina, and E. H. Sargent, *Nature* **442**, 13 (2006).
- ⁵J.-S. Lee, M. V. Kovalenko, J. Huang, D. S. Chung, and D. V. Talapin, *Nature Nano.* **6**, 348 (2011).
- ⁶J. P. Clifford, G. Konstantatos, K. W. Johnston, S. Hoogland, L. Levina, and E. H. Sargent, *Nature Nano* **4**(1), 40 (2009).
- ⁷I. Gur, N. A. Fromer, M. L. Geier, and A. P. Alivisatos, *Science* **310**(5747), 465 (2005).
- ⁸J. M. Luther, M. Law, M. C. Beard, Q. Song, M. O. Reese, R. J. Ellingson, and A. J. Nozik, *Nano Lett.* **8**, 3488 (2008).
- ⁹N. Zhao, T. P. Osedach, L.-Y. Chang, S. M. Geyer, D. Wanger, M. T. Binda, A. C. Arango, M. G. Bawendi, and V. Bulovic, *ACS Nano* **4**(7), 3743 (2010).
- ¹⁰J. Tang, K. W. Kemp, S. Hoogland, K. S. Jeong, H. Liu, L. Levina, M. Furukawa, X. Wang, R. Debnath, D. Cha *et al.*, *Nature Mater.* **10**, 765 (2011).
- ¹¹J. Tang and E. H. Sargent, *Adv. Mater.* **23**, 12 (2011).
- ¹²E. L. Dereniak and G. D. Boreman, *Infrared Detectors and Systems* (Wiley, New York, 1996), p. 306.
- ¹³H. A. Atwater and A. Polman, *Nature Mater.* **9**, 205 (2010).
- ¹⁴K. Catchpole, S. Mokkaṭpati, and F. J. Beck, *MRS Bull.* **36**, 1 (2011).
- ¹⁵K. R. Catchpole and S. Pillai, *J. Appl. Phys.* **100**, 044504 (2006).
- ¹⁶K. Nakayama, K. Tanabe, and H. A. Atwater, *Appl. Phys. Lett.* **93**, 121904 (2008).
- ¹⁷B. P. Rand, P. Peumans, and S. R. Forrest, *J. Appl. Phys.* **96**(12), 7519 (2004).
- ¹⁸F. J. Beck, S. Mokkaṭpati, A. Polman, and K. R. Catchpole, *Appl. Phys. Lett.* **96**, 033113 (2010).
- ¹⁹F. J. Beck, A. Polman, and K. R. Catchpole, *J. Appl. Phys.* **105**, 114310 (2009).
- ²⁰See supplementary material at <http://dx.doi.org/10.1063/1.3678039> for further details.
- ²¹G. Konstantatos, L. Levina, A. Fischer, and E. H. Sargent, *Nano Lett.* **8**, 1446 (2008).
- ²²J. Tang, L. Brzozowski, D. A. R. Barkhouse, X. Wang, R. Debnath, R. Wolowicz, E. Palmiano, L. Levina, A. G. Pattantyus-Abraham, D. Jambakosmanovic *et al.*, *ACS Nano* **4**, 869 (2010).
- ²³F. J. Beck, E. Verhagen, S. Mokkaṭpati, A. Polman, and K. R. Catchpole, *Opt. Express* **19**, A146 (2011).
- ²⁴F. P. García de Arquer, F. J. Beck, and G. Konstantatos, *Opt. Express* **19**, 21038 (2011).
- ²⁵J. D. Jackson, *Classical Electrodynamics*, 3rd ed. (Wiley, New York, 1998), p. 386.
- ²⁶F. J. Beck, S. Mokkaṭpati, and K. R. Catchpole, *Prog. Photovoltaics* **18**(7), 500 (2010).
- ²⁷B. J. Soller and D. G. Hall, *J. Opt. Soc. Am. B* **19**(10), 2437 (2002).